Study of mechanical deformation of $Zr_{55}Cu_{30}Al_{10}Ni_5$ bulk metallic glass through instrumented indentation

A. Rezaee-Bazzaz *, M. Marvi-Mashhadi, M. Haddad-Sabzevar

Department of Metallurgy and Materials Engineering, Faculty of Engineering, Ferdowsi University of Mashhad, Mashhad, Iran

ARTICLE INFO

ABSTRACT

Instrumented sharp indentation experiments using both conical and Vickers diamond pyramidal indenters were carried out to study deformation characteristics of $Zr_{55}Cu_{30}Al_{10}Ni_5$ bulk metallic glass. Finite element simulations of instrumented indentation were also performed to formulate an overall constitutive response. Comparing the experimentally obtained results with the finite element predictions, it can be stated that mechanical deformation of the bulk metallic glass can be described well by both Mohr–Coulomb and Drucker–Prager constitutive criteria. Using these criteria, the extent of material pile-up observed around the indenter was also estimated very well.

© 2011 Elsevier B.V. All rights reserved.

1. Introduction

Bulk metallic glasses have been synthesized by conventional foundry techniques in the early 1990s [1,2]. Since these metallic glasses could be produced in bulk form, the mechanical properties of amorphous alloys became topics of considerable research for possible structural applications. Deformation of bulk metallic glasses differs fundamentally from that of crystalline metals because of the absence of long-range crystallographic order. For uniaxial tests, elastic deformation proceeds catastrophic shear failure that often occurs within a few percent strain after yielding due to shear localization [3–6]. Amorphous metals do not exhibit any strain hardening. Available experimental data strongly suggest that metallic glasses elasto-plastic deformation is influenced by the shear as well as the normal component of local stress, and possibly by the hydrostatic stresses [7,8].

In order to elucidate the multiaxial deformation characteristics of bulk metallic glasses, systematic multiaxial experiments involving different combinations of normal and shear loading are inevitably required. Because of the lack of sufficient quantities of the metallic glasses to prepare specimens of sufficiently large dimensions, and due to the costs and time associated with performing conventional multiaxial mechanical tests, it is difficult to determine multiaxial deformation characteristics of bulk metallic glasses by the conventional mechanical test methods. This difficulty could be circumvented, at least in part, by performing instrumented indentation tests. Using sharp indenters, significant stress fields are created at the contact surface between the indenter and the material leading to flow by activating shear bands in bulk metallic glasses. These constrained deformation tests, unlike the uniaxial tests, do not lead to catastrophic failure and it is possible to study deformation process beyond the elastic domain.

Indentation tests have been extensively used to study bulk metallic glasses. The first aim of using this technique was to characterize the hardness of the alloys and its evolution by the annealing [9] and even the stress-induced crystallization below the indenter [10]. The second aim was the study of load–displacement curves by means of instrumented indentation. In this case, the onset of pop-ins on the curves was correlated with the appearance of shear band around the indenter after unloading [11–14]. Quantitative information about elasto-plastic deformation of bulk metallic glasses can also be extracted from load–displacement curves obtained by instrumented indentation. Elasto-plastic deformation of Zr-based metallic glasses has been studied using instrumented indentation method in some research works. Suresh and co-workers [15] studied mechanical deformation of $Zr_{41.25}Ti_{13.75}Cu_{12.5}Ni_{10}Be_{22.5}$ by instrumented indentation using diamond Berkovich indenter. They found that elasto-plastic deformation of this metallic glass does not follow the Von–Mises criterion and the observed experimental results showed that mechanical deformation of the glass can rather be described by Mohr–Coulomb yield criterion. Ball indentation tests have been conducted for the $Zr_{52.5}Ti_5Cu_{17.9}Ni_{14.6}Al_{10}$ metallic glass by Murty and co-workers [16]. Their work showed that deformation response of this metallic glass is perfectly plastic, strain rate insensitive and pressure independent up to equivalent uniaxial plastic strain of 15%; in contrast to other metallic glasses which show varying degrees of pressure sensitivity. Mechanical deformation of $Zr_{55}Cu_{30}Al_{10}Ni_5$ and $Pd_{40}Ni_{40}P_{20}$ has been studied

* Corresponding author. Tel.: +98 5118763305; fax: +98 5118763305.
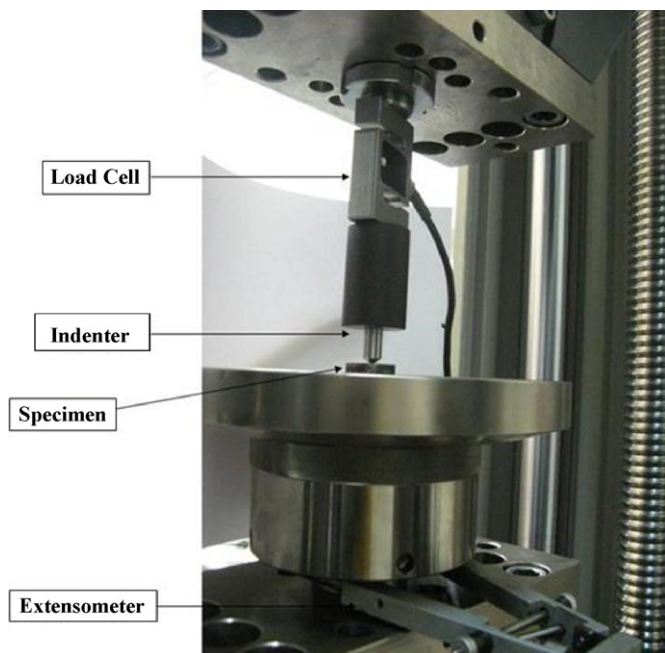*E-mail address:* bazaz-r@um.ac.ir (A. Rezaee-Bazzaz).

Fig. 1. The fixture designed for performing the test by the machine.

by Kryvin using instrumented indentation technique [17]. It was shown that the mechanical deformation of both metallic glasses follows Drucker–Prager yield criterion.

The purpose of the present work was to perform instrumented sharp indentation test on $Zr_{55}Cu_{30}Al_{10}Ni_5$ bulk metallic glass and use computational simulation to determine whether the deformation response of this metallic glass is pressure insensitive, that follows Drucker–Prager criterion or can be described by Mohr–Coulomb yield function.

2. Experimental procedure

2.1. Material and processing

The material investigated in this study was an as-cast fully amorphous $Zr_{55}Cu_{30}Al_{10}Ni_5$ (nominal composition in at.%) alloy. Alloy ingots were prepared by vacuum arc melting of pure metals. The $Zr_{55}Cu_{30}Al_{10}Ni_5$ glassy alloy was made by pouring the molten alloy in a copper mold, which produced cylindrical specimens of 7 mm in diameter. The amorphous nature of the as-cast samples was verified by X-ray diffraction and transmission electron microscopy. Disc shape indentation specimens with a thickness of 2 mm were cut from the rod. The top and bottom surfaces of these specimens were mechanically polished using successive polishing steps (600, 1200, 2400 and 4000 grit papers and 0.1 μm alumina slurry) to obtain flat, mirror-like surfaces.

2.2. Indentation test

The instrumented indentation tests were carried out on a Zwick screw driven computer controlled universal tensile testing machine. The fixture designed for performing the test by the machine is shown in Fig. 1. The lower platen of testing machine was essentially similar to that of the compression test while the indenter was mounted in a holder positioned in the center of the upper platen. During testing, load and indentation depth were continuously measured using a 20 kN load cell and a clip on extensometer, and the data were acquired by a computer. Indentation tests were carried out at a constant crosshead speed of 1 μm/min.

All the indentations were at least 10 mm away from the edges and other indentations. Using the above configuration it was possible to control the load with the accuracy of 0.5 N and to record the indentation depth with the resolution of 0.3 μm. The indents were examined using a roughness tester to study the possible material sink-in/pile-up around the indenter.

3. Finite element computation

Finite element simulation of indentation of the glassy material was carried out in this study. Instrumented indentation using conical indenter has been simulated using axisymmetric reduced elements, while for modeling of indentation by diamond pyramid indenter; three dimensional elements have been utilized. Because of the four-fold rotational symmetry of diamond pyramidal indenter, only a quarter of the material together with indenter has been analyzed.

Computations were performed using the general-purpose finite element package ABAQUS [18], assuming finite deformation characteristics. For the simulation of deformation response of the metallic glass 6859 eight-noded isoparametric solid elements (C3D8) were used in the case of indentation by pyramidal indenter while indentation by conical indenter has been modeled using 676 four-noded quadrilateral axisymmetric reduced elements (C4AXR). Since large deformation takes place near the indenter tip, mesh refinement was accomplished near the contact zone. Three four-noded rigid surface elements (R3D4) were used for simulating a quarter of pyramidal indenter while conical indenter was modeled by the use of an analytical rigid surface. Fig. 2 shows the overall mesh designed for both pyramid and conical indenters. The bottom surfaces were held fixed for both three dimensional and axisymmetric models. Symmetry boundary conditions were applied to the cut faces of the quadrant while the remaining edges were unconstrained in modeling of indentation by pyramidal indenter. In the case of indentation by conical indenter, however, the nodes along the axis of rotation were free to move only along such an axis. To avoid possible convergence problems, small nodal gaps between the specimen and the indenter were defined in both models.

Indentation process was simulated by applying a downward displacement to the rigid body reference node of the indenter. The indentation depth was measured from the displacement of the node situated directly under the indenter tip, i.e., at the point of the first contact. The indentation load for the conical indenter, was the reaction force of the reference node of the rigid indenter, while in the case of indentation by pyramidal indenter, since a quarter of the material and the indenter have been simulated, the reaction force is one-forth of the indentation load.

In this study, Von–Mises continuum plasticity model, Mohr–Coulomb yield criterion and Drucker–Prager yield function were used as elasto-plastic constitutive laws. The Von–Mises yield criterion, where the deformation is assumed to be independent of pressure, is written as:

$$(\sigma_1 - \sigma_2)^2 + (\sigma_2 - \sigma_3)^2 + (\sigma_3 - \sigma_1)^2 = 6k^2 = 2\sigma_y^2 \tag{1}$$

where σ_1, σ_2, σ_3 are principal stresses and $k = \sigma_y/\sqrt{3}$, where σ_y is the yield strength measured in a uniaxial tension test.

The Mohr–Coulomb criterion, where the plastic flow is assumed to be influenced by the local normal stresses, is generally written as [15]:

$$\tau_c = k_0 - \alpha\sigma_n \tag{2}$$

where τ_c is the shear stress on the slip plane at yielding, k_0 and α are constants and σ_n is the stress component in the direction normal to the slip plane.
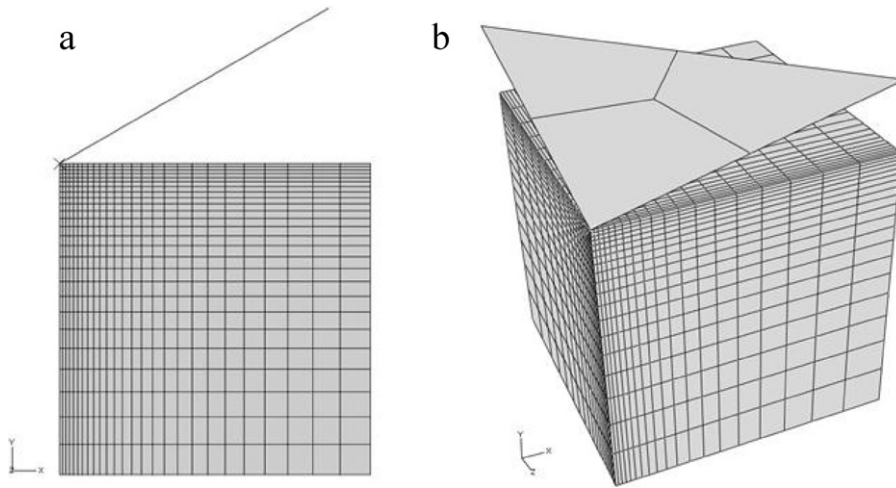
Fig. 2. The overall mesh designed for (a) conical and (b) pyramid indenters.

Drucker–Prager yield surface, in which the plastic flow is assumed to be affected by the local normal stresses, is written in the following form [19]:

$$\frac{1}{6}\left\{(\sigma_1 - \sigma_2)^2 + (\sigma_2 - \sigma_3)^2 + (\sigma_3 - \sigma_1)^2\right\}^{1/2}$$
$$-\alpha_1(\sigma_1 + \sigma_2 + \sigma_3) = k_1 \tag{3}$$

where $\sigma_1, \sigma_2, \sigma_3$ are principal stresses and k_1 and α_1 are two material constants need to be determined experimentally.

When the normal stress dependence coefficients (α in Eq. (2) and α_1 in Eq. (3)) are not zero, plastic flow is non-associated both in Mohr–Coulomb and Drucker–Prager yield function. To ensure the proper and efficient convergence of the computation in this case, a non-symmetric tangent stiffness matrix was used for each iteration.

4. Results and discussions

Fig. 3 shows the results of instrumented indentation experiment of the metallic glass using both diamond pyramidal and conical indenters. Performing finite element simulation requires the knowledge of elastic properties as well as yield strength data of the bulk amorphous metal. Yield strength obtained from uniaxial compression test of $Zr_{55}Cu_{30}Al_{10}Ni_5$ metallic glass has been reported to be equal to 1.8 GPa, and it has also been reported that this metallic glass experiences no strain hardening during plastic deformation [17,20]. Based on experimental data, Poisson's ratio of this metallic glass equals 0.36 [17]. Different elastic moduli of 81.6 GPa [17] and 70 GPa [20] have been reported for the present metallic glass in the literature. A review of the experimental results on other bulk metallic glasses with similar compositions, indicate that elastic moduli of 96 GPa and 89 GPa have been obtained for $Zr_{41.25}Ti_{13.75}Cu_{12.5}Ni_{10}Be_{22.5}$ [15] and $Zr_{52.5}Ti_5Cu_{17.9}Ni_{14.6}Al_{10}$ [16], respectively. Since the value of elastic modulus is not very sensitive to chemical composition, the value of 81.6 GPa has been chosen for elastic modulus of the $Zr_{55}Cu_{30}Al_{10}Ni_5$ in the present investigation.

Based on the above values, indentation load-depth data were predicted by FEM using Von–Mises yield criterion and the results were superimposed on the experimental data in Fig. 3. As the figures show, there is not a good agreement between experimental results and FEM predictions. To use other yield criteria such as Mohr–Coulomb or Drucker–Prager, material constants (k_0 and α for Mohr–Coulomb or α_1 and k_1 for Drucker–Prager) should be determined. For the former criterion, the constants were established so

as to satisfy macroscopic yielding at 1.8 GPa. Dependence of yield strength on normal stress acting on the slip plane necessitates that slip plane deviate from the plane of maximum resolved shear stress in uniaxial compression assuming pressure insensitivity. Taking the effective loading stress as:

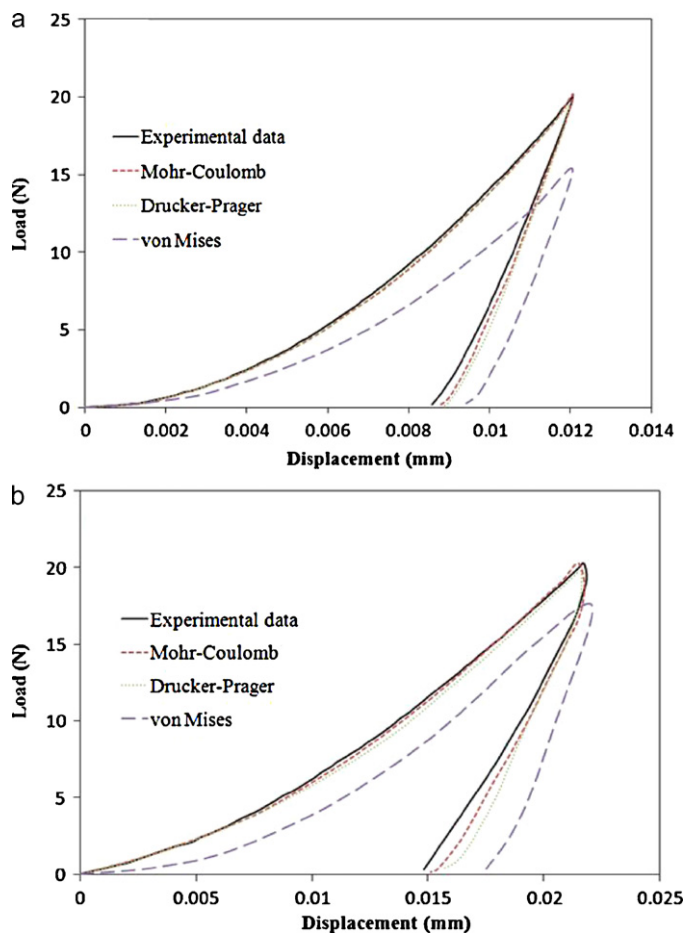$$\tau_{\text{eff}} = \tau_c + \alpha\sigma_n \tag{4}$$

Fig. 3. The results of instrumented indentation experiment of the metallic glass using (a) diamond pyramid and (b) conical indenters.
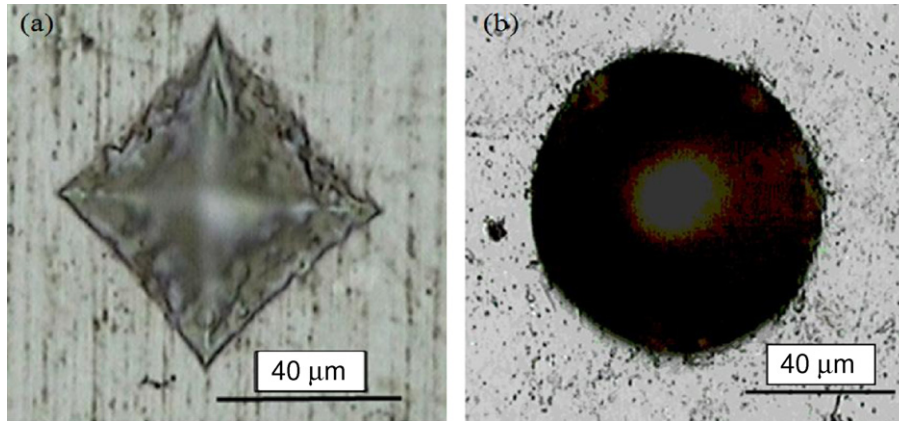
Fig. 4. The optical micrographs of impression using (a) diamond pyramid and (b) conical indenters.

The Mohr–Coulomb yield criterion can be expressed as:

$$\tau_{eff} = k_0 \tag{5}$$

When the specimen is subjected to a uniaxial compressive stress $-\sigma(\sigma > 0)$ Eq. (5) can be written as:

$$\tau_{eff} = \sigma \; \sin\theta \cos\theta - \alpha \sigma \sin^2\theta = k_0 \tag{6}$$

where θ is the angle between the slip plane and the loading axis. Taking the derivative of τ_{eff} with respect to θ gives:

$$\frac{\partial \tau_{eff}}{\partial \theta} = \sigma(\cos 2\theta - \alpha \sin 2\theta) \tag{7}$$

The maximum effective loading stress, τ_{eff}, is obtained when $\partial \tau_{eff}/\partial\theta = 0$ [15]. Obviously, if $\alpha = 0$, solving Eq. (7) results in $\theta = 45°$, which is the angle of the plane with maximum shear stress component assuming pressure insensitivity. Due to the absence of strain hardening, the specimen is expected to experience strain localization as soon as yielding along the slip plane occurs [21]. Observation of a uniaxial compression test specimen of the studied alloy after failure showed that fracture occurs along the plane inclined at an angle approximately equal to 42° with respect to the loading axis [20]. This angle has been reported to be equal to 45° [20] although careful measurement of the angle shown in Fig. 3(a) of this reference shows that the angle is close to 42°. This value is consistent with inclination angle of the failure plane with respect to loading axis reported for $Zr_{41.25}Ti_{13.75}Cu_{12.5}Ni_{10}Be_{22}$ bulk metallic glass [15]. Suresh and co-workers suggested the value of 0.13 for α in predicting indentation load–depth curves of $Zr_{41.25}Ti_{13.75}Cu_{12.5}Ni_{10}Be_{22}$ glass [15]. Considering this value of α and solving Eq. (7) gives $\theta = 41.3°$ which is very close to that measured experimentally. Because the value of θ measured by experiment for $Zr_{55}Cu_{30}Al_{10}Ni_5$ bulk metallic glass is the same as the value obtained for $Zr_{41.25}Ti1_{3.75}Cu1_{2.5}Ni_{10} Be_{22.5}$ glass, the value of 0.13 has been chosen for the studied metallic glass. Choosing θ to be equal to 41.3° for the studied glass, the value of 791 MPa is obtained for k_0 based on Eq. (6). The values of α and k_0 used for $Zr_{55}Cu_{30}Al_{10}Ni_5$ bulk metallic glass in this study differ from those used for the same glass by Keryvin [17]. Predicting indentation load–depth curves by FEM and using Mohr–Coulomb yield function assuming the above values for α and k_0, and superimposing the results on the experimental data in Fig. 3 shows a good correlation between the predicted and experimental results.

If the material constants for Mohr–Coulomb yield criterion have already been determined, it is possible to use Drucker–Prager yield function instead of Mohr–Coulomb yield surface to eliminate sharp corners in yield loci. Drucker–Prager material constants can be determined by coinciding Drucker–Prager circular cone with the outer apexes of the Mohr–Coulomb hexagon at any section. Therefore, the following relationship between Drucker–Prager material constants and those of Mohr–Coulomb yield criteria obtains [19]:

$$\alpha_1 = \frac{2\sin \; (\tan^{-1}\alpha)}{\sqrt{3} \left(3 - \sin \left(\tan^{-1}\alpha\right)\right)} \tag{8a}$$

$$k_1 = \frac{6k_0 \cos \left(\tan^{-1}\alpha\right)}{\sqrt{3} \left(3 - \sin \left(\tan^{-1}\alpha\right)\right)} \tag{8b}$$

Substituting the values of α and k_0, determined for Mohr–Coulomb criterion, into the above equations, the values of material constants for Drucke-Prager yield function are found to be $\alpha_1 = 0.052$ and $k_1 = 946.416$ MPa. Using these material constants, indentation load–depth curves were predicted by FEM. The predicted results are superimposed on the experimental data in Fig. 3. Comparison of the predicted and experimental results shows a good agreement between predictions and experimental results.

Fig. 4(a) and (b) shows optical micrographs of impression using pyramidal and conical indenters, respectively. As these figures show, nothing but the imprint is observed in the micrographs of the impressions produced by both conical and diamond pyramidal indenters which agrees with those reported by Keryvin [17]. It is noteworthy that the formation of shear bands around the impression made by a conical indenter under loads greater than 150 N has been reported by Keryvin. In the present investigation, with a maximum load was 20 N, no shear bands were observed around the impression. The formation of shear bands around indentation imprints in Zr-based glasses made by Vickers diamond indenter has also been reported in the literature [17].

Suresh and co-workers [15] showed that the position of shear bands around the indenter correlates with the normalized effective stress and these bands locate at positions where this normalized effective stress reaches the value of one. In order to find the reason for the lack of shear bands around the indenter imprint in this study, distribution of the normalized effective stress for the indentation of the studied glass using both conical and pyramidal indenters were examined. Fig. 5(a)–(c) show the normalized effective stress distribution on the surface of the specimen subjected to indentation by diamond pyramidal indenter after unloading and using Von–Mises, Mohr–Coulomb and Drucker–Prager yield criteria, respectively. Fig. 6(a)–(c) show the distribution of aforementioned quantity on the surface of the specimen subjected to indentation by conical indenter after unloading and using each of the proposed yield functions. It is noteworthy that the normalized effective stress for each of the yield criteria is defined by dividing the left hand side of Eqs. (1), (3) and (5) by the their respective right
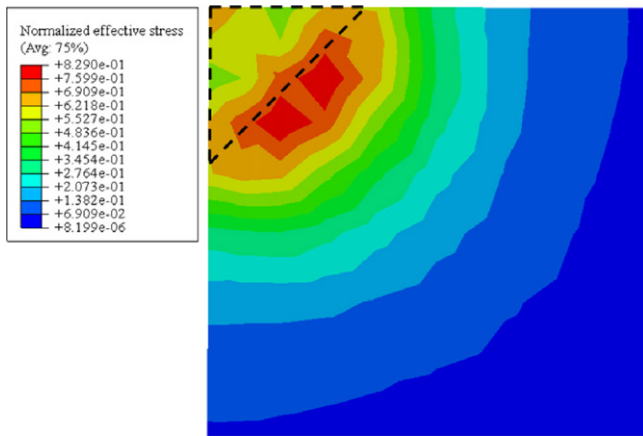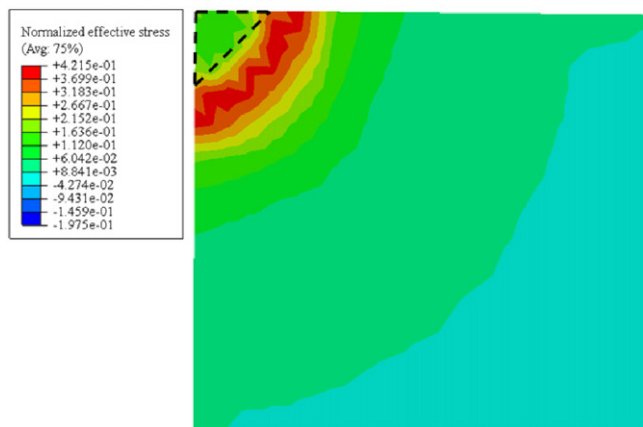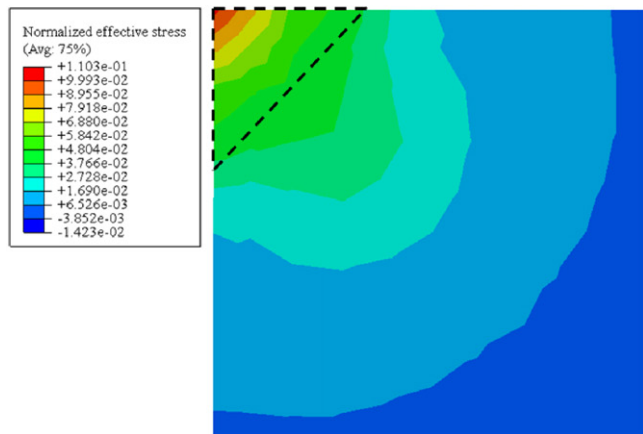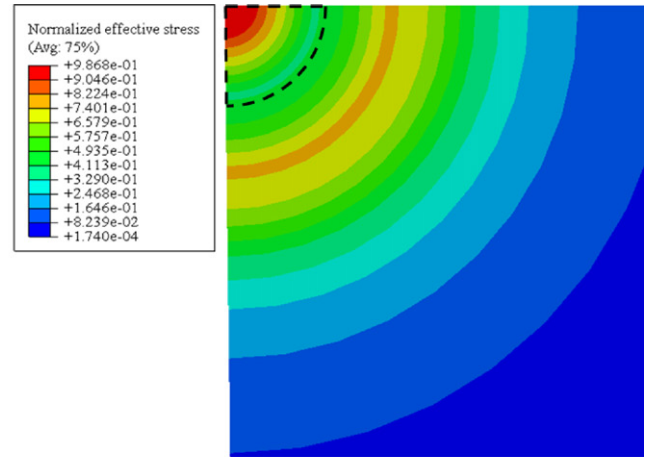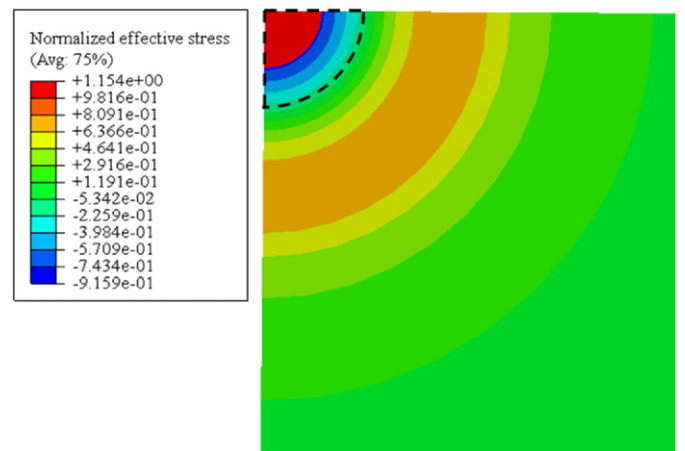
Fig. 5. Normalized effective stress distribution on the surface of the specimen subjected to indentation by diamond pyramid indenter using (a) Von–Mises, (b) Mohr–Coulomb and (c) Drucker–Prager yield criteria.

Fig. 6. Normalized effective stress distribution on the surface of the specimen subjected to indentation by conical indenter using (a) Von–Mises, (b) Mohr–Coulomb and (c) Drucker–Prager yield criteria.

hand side. Taking a look at these figures, it is clear that the normalized effective stress never reaches the value of one in indentation by diamond pyramidal indenter and this quantity reaches the value of around one in indentation by conical indenter at the position located beneath the indenter. Therefore, using FEM simulation of instrumented indentation of the studied glass, the lack of shear bands around the indenter is predictable.
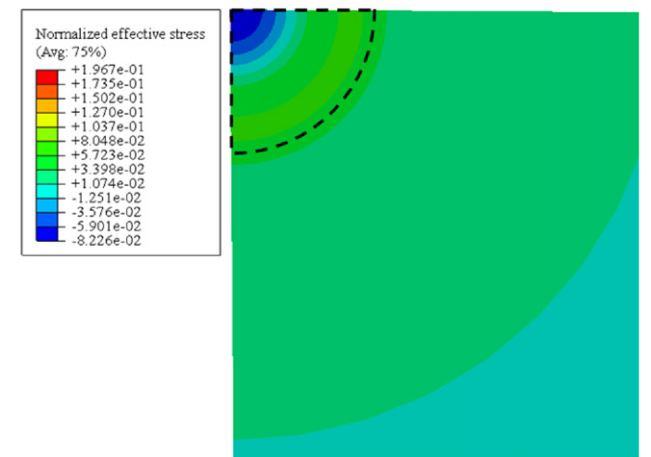
Fig. 7(a) and (b) shows a comparison between experimentally determined surface profile of the indentation imprint and those obtained from FEM simulations for both diamond pyramidal and conical indenter. As it is clear from these figures, both Mohr–Coulomb and Drucker–Prager yield criteria are able to estimate well the surface profile of the studied glass indentation. Therefore, using FEM and by the use of either Mohr–Coulomb or Drucker–Prager yield criteria, the material pile up around the indentation can be well predicted.
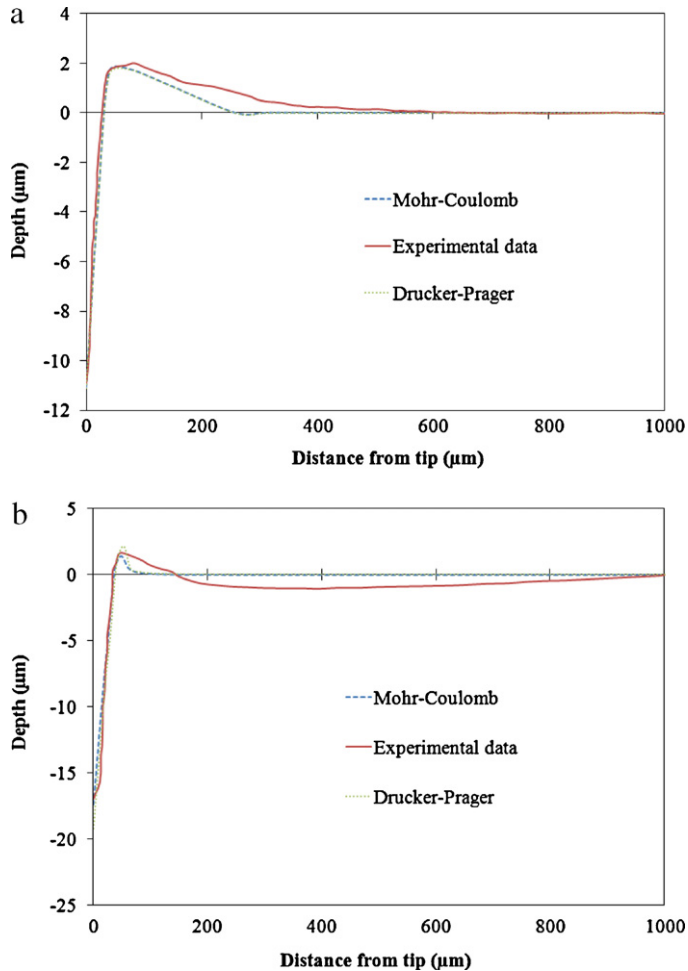
Fig. 7. Surface profile of the indentation imprint for (a) diamond pyramid and (b) conical indenter.

5. Conclusions

Doing instrumented indentation of $Zr_{55}Cu_{30}Al_{10}Ni_5$ bulk metallic glass using sharp indenters and simulating this experimental technique, the following conclusions are made:

1. Comparison of the experimental load–depth curves with those predicted by FEM simulations shows that the studied material does not follow the Von–Mises yield criterion. The obtained experimental results are consistent with FEM simulations using both Mohr–Coulomb and Drucker–Prager yield criteria; suggesting the influence of normal stress components on plastic deformation of the glass.
2. The FEM predictions using both Mohr–Coulomb and Drucker–Prager can successfully simulate pile up around the indenter after unloading.
3. There is no difference between predictions made by Mohr–Coulomb or Drucker–Prager yield criteria. Therefore at least for simulating indentation of the studied glass, either Mohr–Coulomb or Dracker-Prager yield criterion can be used with equal confidence.

References

[1] A. Inoue, T. Zhang, T. Masumoto, Mater. Trans. JIM 31 (1990) 177–183.
[2] A. Peker, W. Johnson, Appl. Phys. Lett. 63 (1993) 2342–2344.
[3] W.L. Johnson, Mater. Res. Bull. 24 (1999) 42–56.
[4] A. Inoue, Acta Mater. 48 (2000) 279–306.
[5] Z.F. Zhang, J. Eckert, L. Schultz, Acta Mater. 51 (2000) 1167–1179.
[6] C.T. Liu, L. Heatherly, D.S. Easton, Metall. Mater. Trans. A 29 (1998) 1811–1820.
[7] P.E. Donovan, Acta Metall. 37 (1989) 445–456.
[8] P. Lowhaphandu, S.L. Montgomery, J.J. Lewandowski, Scripta Mater. 41 (1999) 19–24.
[9] M.L. Vailant, V. Keryvin, T. Rouxel, Y. Kawamura, Scripta Mater. 47 (2002) 19–23.
[10] J.J. Kim, Y. Choi, S. Suresh, Science 295 (2002) 654–657.
[11] Y. Golovin, V. Ivolgin, V. Khonik, K. Kitagawa, A. Tyurin, Scripta Mater. 45 (2001) 947–952.
[12] C. Schu, A. Argon, T. Nieh, Philos. Mag. 83 (2003) 2585–2597.
[13] C. Schu, T. Nieh, Acta Mater. 51 (2003) 87–99.
[14] L. Liu, K. Chan, Mater. Lett. 59 (2005) 3090–3094.
[15] R. Vaidyanthans, M. Dao, G. Ravichandran, S. Suresh, Acta Mater. 49 (2001) 3781–3789.
[16] G.R. Trichy, R.O. Scattergood, C.C. Koch, K.L. Murty, Scripta Mater. 53 (2005) 1461–1465.
[17] V. Keryvin, Acta Mater. 55 (2007) 2565–2578.
[18] ABAQUS, General purpose finite element program, Version 6.4, Hibbit Karson and Sorensen Inc, Pawtucket, RI, 2003.
[19] A.S. Khan, S. Huang, Continuum Theory of Plasticity, John Wiley & Sons Inc., 1995.
[20] M. Heilmair, J. Mater. Proc. Technol. 117 (2001) 374–380.
[21] R.J. Asaro, J.R. Rice, J. Mech. Phys. Solids 25 (1977) 309–338.